Achievements in the Development of Space-borne Imaging Radar

Yunjin Kim, Fred Stuhr, Jakob van Zyl, Paul Rosen,
Anthony Freeman, William Johnson, Rolando Jordan, Ed Caro, and Yuhsyen Shen
Jet propulsion Laboratory
California Institute of Technology
4800 Oak Grove Drive
Pasadena, California 91109-8099

ABSTRACT

This article describes past and current achievements in the development of space-borne imaging radar technology and discusses possibilities for the future. The article focuses on space-borne capabilities for civil and scientific purposes. The history is recounted over the past 50 years of radar imaging evolution from airborne research systems to operational space capabilities. Radar's ability to "see" through darkness, clouds and smoke and to cover large areas give it unique power as a global remote-sensing tool. Operational space-borne systems of today are capable of generating global geological and topographic maps, using advanced synthetic aperture radar (SAR) techniques such as polarimetry and interferometry. One of the most promising remote sensing capabilities is SAR interferometry, which produces three-dimensional images and permits measurement of mm-level surface displacement at high resolution. Future space-borne imaging radar developments are aimed at enabling more affordable missions by reducing flight system mass and power. The future holds great promise for increased use of radar for remote sensing, including more accurate elevation mapping, natural hazards monitoring, soil moisture mapping and biomass estimation.

I. INTRODUCTION

Imaging radar refers to systems and techniques for collecting and processing two-dimensional arrays of radar backscatter data. Imaging radar has evolved from the rudimentary target location systems of post-World War II to sophisticated space-borne imaging capabilities. Radar's capability to "see" through darkness, clouds and smoke and to cover large areas rapidly from space make it a powerful remote sensing tool for a variety of potential civil, military, scientific and commercial applications [1]. A number of missions using imaging radar have been flown and are now flying to produce valuable radar imaging data from space for benefits on earth [2,3]. Radar missions to distant planets are providing data for planetary science, such as the unprecedented surface details through the dense cloud cover of Venus.

Technology developments in flight radar equipment, processing capabilities and remote sensing techniques have made space-borne imaging radar systems possible. Flight equipment progress includes higher power, wider bandwidth, larger antennas and increased frequency and phase stability. Processors have evolved to extremely high rate digital systems. During the past decade, two powerful synthetic aperture radar (SAR) techniques emerged: polarimetry and interferometry [4,5]. Especially, the use of interferometry to measure height and height changes is one of the most promising radar capabilities. It allows the production of three-dimensional images and very precise measurement of surface change [6]. Highly accurate digital elevation maps over very large areas can be produced in significantly less time and at significantly lower cost with radar than with other systems. Many geological and ecological studies using radar data were enabled by SAR polarimetry. Most future radar missions will be designed for dedicated science objectives by utilizing advanced radar techniques.

Space-borne imaging radar programs for civil and scientific purposes are active in many countries around the world. These programs are typically led by the government space agencies working in partnership with industry, universities and research institutions. The U.S. National Aeronautics and Space Administration (NASA) imaging radar program, conducted by the Jet Propulsion Laboratory (JPL), spans the last 30 years and includes planetary and earth missions. These NASA missions have often included cooperative efforts with international partners, including Germany and Italy, as well as industry. Four radar imaging satellites were launched in the 1990's by the European Space Agency (ESA), the Japanese National Space Development Agency (NASDA) and the Canadian Space Agency (CSA). The Soviet Union used SAR for several Earth-orbiting missions as well as a pair of imaging radars to Venus in 1983.

This article first describes the early radar development, profiling the evolution to space-borne imaging radar. The advanced radar techniques that have enabled radar remote sensing applications are outlined. In order to describe the progress in radar remote sensing, past radar missions from the Apollo Lunar Sounder to the Shuttle Radar Topographic Mission to be launched in September 1999, are summarized. Finally, potential future radar missions and their characteristics are discussed.

II.EARLYDEVELOPMENT

Imaging radar was non-existent 50 years ago. Although Hertz demonstrated the principle that radio waves can be reflected off objects as early as 1886, radar developed very slowly until World War II. The word "radar" was a code-name used by the U.S. Navy in 1940 for *ra*dio *d*etection *a*nd *r*anging. Radar systems in the early development were ground or ship based and used large, heavy equipment and rudimentary processing. These radars detected objects and provided information as to position relative to the radar over time.

Following World War II, aircraft served as radar platforms for the development of imaging. These aircraft flew with the radar antenna boresight perpendicular to the direction of motion, to produce a two-dimensional array of backscatter data. These systems were known as side-looking airborne radars (SLAR). These imaging radars transmitted pulsed signals and used time delay of returns as the measure of range to the target. The aperture for each image "frame" consisted of the antenna illumination area on the ground. Within a "frame", the resolution in the across-track direction was proportional to the radar pulse duration and the resolution in the along-track direction was proportional to the antenna beamwidth. An image swath was formed by assembling frames as the aircraft flew along. Higher across-track resolution was achieved by increasing the transmitted signal bandwidth. Higher along-track resolution was achieved by longer antennas for relatively low flying aircraft. Pulse compression technique developments continued to enhance resolution capabilities for the across-track direction, independent of altitude. The physical constraints of these "real" aperture imaging radars severely limited the along-track resolution for space-borne platform altitudes.

Carl Wiley of Goodyear Aircraft Corporation theorized the SAR technique in 1951 [7]. The Doppler information in the echo returns is used simultaneously with the time-delay information to generate an image of much higher resolution in the along-track direction than the area illuminated by the antenna. SAR imaging was demonstrated aboard aircraft in the late 1950's.

One unique feature of the synthetic-aperture imaging radar process is that its resolution is independent of the altitude of the platform. This unique capability allows the acquisition of high-resolution images from space, as long as there is sufficient received signal-to-noise ratio (SNR). This advancement set the stage for space-borne imaging radar.

A number of key developments enabled space-borne radar flight systems to collect SAR data. This includes capabilities for wider bandwidths and increased pulse compression. Extremely stable local oscillators were developed, which allow the coherency of the starting phase of each pulse to be maintained. This allows the system to preserve the Doppler information required for forming the radar synthetic aperture. Development of higher power amplifiers, such as the traveling wave tube (TWT), provided increased SNR. Phased array antennas, with numerous transmit & receive (T/R) modules, provided increased sensitivity and reliability and allowed electronic beam-steering. Improvements in deployable structures enabled larger antennas. The first successful SAR data processor was an optical correlator, using photographic film. Digital processing was in use by the late 1970s. Currently, all SAR processors are fully digital through developments in digital computer technology.

III. SPACE-BORNE SAR MISSIONS

A. Apollo Lunar Sounder Experiment

The first planetary synthetic aperture radar system was flown on the Apollo 17 spacecraft around the moon in 1972. This sensor was called the Apollo Lunar Sounder [8] and it was specifically designed for subsurface sounding of the lunar crust. One of its three frequency channels (150 MHz) was able to acquire SAR imagery at a 2-meter wavelength using a side-looking Yagi antenna.

B. SEASAT, SIR-A, and SIR-B Synthetic Aperture Radar

The first civilian space-borne SAR system specifically designed to acquire high-resolution images of the Earth surface was the SEASAT SAR launched by NASA in 1978. It represented the state of the art in sensor technology in the late 1970's. This system was subsequently modified and flown on two space shuttle flights as the SIR-A instrument in 1981 and SIR-B in 1984 [9,10].

The SEASAT SAR system consisted of a planar array antenna, the radar sensor, an analog data link, a data formatter and a high-density digital recorder. The planar array antenna, the

radar electronics and an analog transmitter were located on the spacecraft. On the ground was a down converter with a synchronous demodulator, the analog to digital converter and digital recorder. Processing of the digital signals to imagery was done by first converting the digital signal output to an optical format on high-resolution film and processing the optically recorded signals to images using an optical correlator. Subsequently, a digital processor was developed to directly process the digitally recorded data to images without going through the optical correlation process.

The SEASAT SAR system operated successfully for 100 days and acquired approximately 50 hours of radar data. The spare hardware of the SEASAT radar system was then modified and flown on the Shuttle in November 1981 as the SIR-A experiment. The modifications to the SEASAT hardware were to reduce the bandwidth and remove one of the panels of the antenna. The horizontal polarization antenna was mounted at a fixed 50-degree look angle with the data recorded on a modified Apollo Lunar Sounder optical recorder. Since the recorder was located in the Shuttle payload bay, only a single roll of film was used but it allowed data acquisition for seven and one-half hours. The SEASAT SAR system operated at a fixed 20.5 degree look angle from the spacecraft while the SIR-A system had a 50-degree look angle from the Shuttle. The SIR-B system was then modified and flown in 1984 incorporating a steerable antenna over a 20 to 60 degree range. The polarization of the antenna was horizontal polarization.

C. Magellan

The concept of an imaging radar mission to Venus, using SAR to peer through the dense cloud cover, was first put forward in the late 1960's. The scientific objectives for a NASA SAR mission were established in a 1972 study, which defined a radar imaging mission patterned after the optical imaging of the Mariner 9 Mars mapping mission. This proposed mission, known as the Venus Orbiting Imaging Radar (VOIR), was deemed too costly. A scaled-down mission, with only radar (imaging, altimetry, and radiometry) and Doppler gravity experiments, was designed in 1982. The redesigned mission, known as Magellan, was launched from the space shuttle Atlantis in 1989. Magellan followed Earth-based radar studies and two previous orbiting radar missions, Pioneer Venus Orbiter in 1978 and the Soviet Union's Veneras 15/16 in 1983.

The design of the Magellan radar system [11] used data from previous missions, but was constrained in many ways by the choice of spacecraft and its orbit. The elliptical orbit and small antenna (compared to what Earth-orbiting SAR's normally use) present the radar with a challenging environment. The design must use each of the limited resources (especially the

downlink data rate) efficiently, so that the mission can complete its primary objectives in one rotation of the planet (243 Earth days). The radar is also used as an altimeter and a radiometer. Between SAR bursts, typically several times a second groups of altimeter pulses are transmitted from a dedicated fan-beam altimeter antenna directed toward the spacecraft's nadir. The Magellan Mission met all of its requirements and most ambitious goals. The imaging coverage requirement of 70% was surpassed with 98% coverage. Similar successes were achieved for the altimetry and radiometry coverage. In Fig. 1, we show one full resolution Magellan image of three large impact craters with diameters ranging from 37 km to 50 km. This Magellan image resolution is about 120m.

D. SIR-C/X-SAR System

The Spaceborne Imaging Radar-C / X-band Synthetic Aperture Radar (SIR-C/X-SAR), a joint US/German/Italian project, was the first spaceborne multi-frequency, multi-polarization imaging radar [12]. The mission aboard the shuttle Endeavour consisted of a 10-day flight in April 1994 and a second 10-day flight in October 1994, each at an altitude of about 225 km. Data "takes" were largely over experiment sites selected prior to launch. The second flight provided the opportunity for assessment of change with time due to seasons and other factors. Also, the orbit was trimmed for the last three days of the second flight to nearly repeat the track of the first flight. This allowed interferometric processing of the pairs of data sets. For the two flights, a total of 143 hours (93 terabits) of SAR data were digitally tape-recorded on 360 tapes onboard the Shuttle for post-flight ground processing.

The NASA SIR-C used an active phased array antenna, which allowed boresite steering and beamwidth adjustment in elevation. The German/Italian X-SAR used a slotted waveguide antenna, mechanically steerable in elevation. The three antenna apertures shared the same along-track lengths of 12 m. This produced azimuth pattern beamwidth ground coverage proportional to wavelength and allowed the same pulse repetition frequency (PRF) for all three frequencies. The antenna apertures physically shared the 4.2-m across-track dimension proportional to wavelength. This produced approximately equal across-track ground coverage for all the frequencies. The SIR-C/X-SAR system and antenna support structure weighed approximately 20,000 pounds and used up to 9 kW of Shuttle power when operating. While the SIR-C electronics equipment was conservative in construction, the overall radar capability is significantly advanced. The multiple elements of the phased array antenna, the redundancy in the sensor electronics, and multiple data routing paths gave SIR-C significant failure tolerance.

SIR-C and X-SAR were effectively five separate radars with regard to frequency and polarization. SIR-C operated at 1250 MHz (L-band) and 5300 MHz (C-band) with up to four simultaneous transmit/receive polarizations (VV, VH, HV, VV), while X-SAR operated at a single 9600 MHz (X-band) frequency with VV polarization. With the amplitude of four polarizations and the relative phase between them, the complete scattering matrix of a scene can be derived on a pixel-by-pixel basis. The SIR-C active phased array provided the sensitivity to detect weak cross-polarization echoes, while maintaining acceptable transmit power levels, by locating the transmit amplifiers and receivers next to the antenna radiating elements.

The SIR-C phased array enabled operation in modes known as SCANSAR and SPOTLIGHT. For SCANSAR, the antenna beam was stepped across-track during the synthetic aperture period. A wider swath is accomplished at the expense of azimuth resolution. For SPOTLIGHT, the boresight was re-positioned in azimuth as the Shuttle flew by to dwell on the same area. This allowed an increase in azimuth resolution to as small as 7 m for the selected area, at the expense of the along-track swath.

Repeat-track interferometric data were obtained at all three SIR-C/X-SAR frequencies, with across-track interferometric baseline separations of 10 to 4700 m. Day-to-day repeats were accomplished during the second flight as well as 6 months repeats between flights. SIR-C also had an along-track interferometric mode for detection of motion in the azimuth direction. This mode was achieved by simultaneously operating the outermost six C-band panels at each end as separate antennas. One SIR-C image is shown in the advanced technique section.

E. Cassini Radar

The Cassini spacecraft, launched in October 1997, carries a multimode Ku-band (13.8 GHz) radar instrument (RADAR) designed to probe Titan's surface and other targets in the Saturn system [13]. The radar was a cooperative effort by the U.S. and Italy. It is distinguished by a number of novel features which accommodate the large geometric variations in flyby trajectories and the wide range of uncertainty in surface properties and which efficiently utilize the limited spacecraft resources such as the data rates, the data volumes, and power. The overall science objectives of the Cassini mission include five Titan-specific objectives. Two of these—the determination of the physical state, topography, and composition of the Titan's surface; and the measurement of global temperatures and general circulation on Titan—constitute the overriding goal of the RADAR experiment. Whenever feasible, the RADAR will also conduct observations of the icy satellites, Saturn's rings, and Saturn itself. The Titan observations,

however, constitute the highest scientific priority for the RADAR, and they drive its design. The instrument was designed to incorporate four modes: imaging (either high- or low-resolution), altimetry, scatterometry, and radiometry.

The high-resolution (350 to 720 m) SAR images will permit identification of features and terrain types on Titan and in different viewing geometries. RADAR scatterometer data will reveal the backscatter efficiency vs. incidence angle for a large fraction of Titan' surface, although the spatial resolution may be coarse. Nonetheless, scatterometer data will constrain surface slope distribution and the density of the uppermost decimeter of the surface. Scatterometer data will also be most similar to the data taken with the upgraded ground radar at Arecibo, Puerto Rico during the coming decade and therefore will allow Titan's global radar properties to be defined in detail.

Tight constraints on mass and volume required that the RADAR share the 4-m telecommunications antenna (HGA), as did the radar on the Magellan mission. The system design also dictated that a single feed or beam could not meet the per-flyby requirements of imaging and other modes simultaneously. A five-feed, five-beam design was decided upon, in which the center, highest-gain beam would be used in all modes. The additional four beams would be used in the imaging mode, creating a wide swath. Beam switching would be done inside the RADAR.

The RADAR lacks opportunity to acquire processable echoes prior to its first data-collecting flyby of Titan, likely to take place in 2005. Radar-operational flybys of Venus and Earth will allow the first closed-loop test of the RADAR system. As helpful as these tests are, they would still simulate operations at targets vastly different from Titan. Little is known about the surface characteristics of Titan. Even less is known about the performance of the RADAR radiometer and about the thermal effect of a 10-hour RADAR flyby of Titan on the performance of the spacecraft systems.

F. Shuttle Radar Topography Mission

The Shuttle Radar Topography Mission (SRTM) is capable of producing a three-dimensional image of 80% of the Earth's land surface in a single 10-day Space Shuttle flight [14]. It is the first spaceborne single-pass interferometric SAR and will produce the first near-global, high-resolution, digital elevation map. Repeat-pass must contend with decorrelation, which increases with the operating frequency. Such a global map will be constructed significantly sooner

than with other systems by taking advantage of the unique opportunity offered through augmentation of the previously flown NASA SIR-C and theX-SAR. Addition of a C-band receive antenna, extended from the Shuttle bay on a mast and operating in concert with the existing SIR-C antenna, forms an interferometric pair. Due to the practical limitation of approximately 60 meters for the mast length, the shorter C-band wavelength produced greater height accuracy than with the SIR-C L-band. C-band allowed a smaller antenna, which was more manageable for the mast. The data channels, previously used for L-band, could be used to support the added interferometric receive channels through frequency conversion. The existing SIR-C SCANSAR mode, combined with the dual-polarization capability, allowed a 225-km swath at C-band. This provided complete land coverage within 57 degrees north and south latitude. IFSAR measurements will also be obtained by the German/Italian X-SAR, utilizing an added outboard antenna at X-band to produce swath coverage of about 50 km. It is estimated that the achievable height accuracy is less than 16 meters absolute and 11 meters relative, where these values are the 90% linear error after processing both ascending and descending passes. The elevation postings are 30 meters.

The outboard C- and X-band receive antennas are mounted on a support structure, which is fastened to the end of the mast. The mast is composed of graphite epoxy struts connected by metallic hinges and supported by locking wire stays in the extended configuration. The mast is stored for launch in a 1.4 X 3 m cylindrical canister and the outboard support structure is latched to the outside of the canister. The mast extends 60 meters length. The C-band antenna array consists of 12 panels, each of which has an identical radiating patch design as the inboard SIR-C transmit/receive antenna to enhance the common beam and steering characteristics required. The receive antenna is populated with low-noise-amplifiers (LNAs) and phase shifters for both horizontal and vertical polarization beams. The two antenna beams are required to continuously cover the same ground area. Open loop pointing requires that the antenna mechanical motion be within stringent limits. In order to insure that the beams are aligned, a capability was added to automatically steer the outboard receive beam to track the inboard transmit beam in azimuth. The beam auto-tracker can steer the beam to within 10% of the outboard receive antenna beamwidth.

Since the relative phase of the two interferometric channels is the basis for height determination, the stability of the intervening receive paths through the antennas to the common receive point is critical. A capability added for SRTM was the in-flight measurement of the receive path phase variations for correction during processing. This measurement was implemented using calibration signals generated by the radar and injected into the receive paths at the antennas. The approximately 60-meter length of the cabling in the injection path to the outboard antenna presented a

problem due to its uncalibrated phase variations. Hence, a closed loop optical link was implemented, which maintained a constant phase at the outboard injection point.

In addition to the radar augmentations, a metrology capability was implemented for the interferometric operation to:

1) measure the baseline characteristics
2) determine the position of the shuttle relative to the Earth
3) provide a precise time base for all data.

A star tracker and an inertial reference unit measure the baseline attitude. The relative motion of the outboard antenna is monitored, as is the distance between the inboard and outboard platforms, by two other sensors. The Global Positioning System (GPS) is used to determine the position of the Shuttle and to provide the time base.

G. International SAR Satellites of the 1990's

The international use of spaceborne imaging SARs for long-term Earth observation dramatically increased in the 1990's. While the U.S. NASA missions were Shuttle-based, there are four SAR imaging satellites operated by the Europeans, Japanese and the Canadians. These satellites transmit the data to Earth at tracking stations distributed throughout the world. The data are then processed at central processing facilities in Europe, Japan, Canada and the U.S.

The European Space Agency (ESA) launched a SAR aboard the European Remote-Sensing Satellite (ERS) in August 1991 and another in April 1995 [15]. Each ERS employs a C-band SAR operating at a fixed look angle of 23 degrees and with VV polarization. The antenna is a 10 m x 1 m planar waveguide array and the transmitter utilizes a Travelling Wave Tube Amplifier. The swath is 100 km and the resolution is 24 m. Global land and ocean coverage have been provided by ERS-1 and 2. Of particular note to scientists are the arctic ice coverage products. Multiyear, time-sequenced data depict the polar ice pack motion, ice thickness and glacier motion. Pairs of ERS images, including tandem ERS-1/2, have been used to generate interferometric data products of surface topography and surface deformation. These data are especially useful for analyzing post-seismic events and detecting surface deformations associated with volcano pre-eruptions.

The National Space Development Agency (NASDA) launched a SAR aboard the Japan Earth Resources Satellite (JERS-1) in February 1992 [16]. JERS employs a L-band SAR operating at a fixed look angle of 35 degrees and with HH polarization. The swath is 75 km and

the resolution is 18 m. JERS has provided gobal landcover mapping. Significant JERS products include a digital map database of the South America rainforests, which are often cloud-covered. Repeat-pass interferometric data have been used to measure surface deformations on the order of mm.

The Canadian Space Agency launched a SAR aboard RADARSAT in September 1995 [17]. RADARSAT employs a C-band SAR capable of multiple modes. The antenna is a 1.5 m x 15 m planar slotted waveguide array. Ferrite variable phase-shifters are employed for electronic beam steering, which is a key feature. The transmitter utilizes two Travelling Wave Tube Amplifiers for redundancy. The amplifiers are derived from those developed for ERS. The RADARSAT modes include a variety of swath widths and resolutions. A fine resolution mode is capable of 9 m resolution over a 49 km swath. The use of SCANSAR allows swath coverage as wide as 500 km, with resolution as good as 40 m, to achieve very large area mapping.

RADARSAT has provided global SAR products for commercial and scientific customers. RADARSAT International distributes data to the commercial users. Arctic ice coverage products have been utilized for ship operations and for research of sea ice motion. The RADARSAT Antarctic Mapping Project (RAMP) has mapped Antarctica providing provide critical benchmarks for gauging future changes in the extent, the shape, and the dynamics of the great Antarctic Ice Sheet. It will also contribute to the understanding of iceberg formation and the geologic history of the Antarctic continent.

IV. ADVANCED TECHNIQUES

A. SAR Polarimetry

Electromagnetic wave propagation is a vector phenomenon, so that measurement of the complete complex scattering matrix is necessary to completely characterize the scattering properties of terrain. The typical implementation of a radar polarimeter involves transmitting a wave of one polarization and receiving echoes in two orthogonal polarizations simultaneously. This is followed by transmitting a wave with a second polarization, and again receiving echoes with both polarizations simultaneously. In this way, all four elements of the scattering matrix is measured. The NASA/JPL AIRSAR system pioneered this implementation for SAR systems [18], and the same implementation was used in the SIR-C part of the SIR-C/X-SAR radars [12].

Many of the advances made in analyzing polarimetric SAR data result directly from the

greater availability of calibrated data. Polarimetric calibration usually involve four steps: cross-talk removal, phase calibration, channel imbalance compensation and absolute radiometric calibration [19]. Cross-talk removal refers to correcting mostly the cross-polarized elements of the scattering matrix for the effects of system cross-talk that couples part of the co-polarized returns into the cross-polarized channel. Phase calibration refers to correcting the co-polarized phase difference for uncompensated path length differences in the transmit and receive chains, while channel imbalance refers to balancing the co-polarized and cross-polarized returns for uncompensated gain differences in the two transmit and receive chains. Finally, absolute radiometric calibration involves using some kind of a reference calibration source to determine the overall system gain to relate received power levels to normalized radar cross-section [20].

B. SAR Interferometry

The remote sensing technique referred to as Interferometric Synthetic Aperture Radar (InSAR, sometimes termed IFSAR or ISAR) has grown tremendously in popularity over the past two decades. A conventional SAR only measures the along-track and cross-track location of a target, projecting topographic relief information into a two-dimensional imaging plane. Often this altitude-dependent distortion limits the ability to interpret the imagery. InSAR techniques have developed to measure the third dimension, and have given rise to a variety of new technologies and applications.

Graham [23] augmented a conventional SAR system with an additional physical antenna displaced in the cross-track plane from the conventional SAR antenna, forming an imaging interferometer. The Graham interferometer mixed the signals from the two antennas, recording amplitude variations that represented the beat pattern of the relative phase of the signals. The relative phase changes with the topography of the surface, so the fringe variations tracks the topographic contours.

InSAR systems were developed subsequently to record the complex amplitude and phase information digitally for each antenna. In this way, the relative phase of each image point could be reconstructed directly. Zebker and Goldstein [24] first demonstrated such a system on an airborne platform. Li and Goldstein [25] demonstrated the capability from a spaceborne platform using SeaSAT data acquired on different days. Presently, over a dozen airborne interferometers exist throughout the world, generating fine resolution digital elevation models at 1-10 m postings, and 20cm to 2 m vertical accuracy.

With the launch of ERS-1 and JERS-1 in 1992, SIR-C/X-SAR in 1994 for two 10 day missions, and RadarSAT-1 in 1995, and with increased availability of SAR data, spaceborne SAR interferometry is now extremely popular. The interferometer is formed by combining images obtained at different times on repeated passes over an area on the Earth. If the surface does not move between observations, and if the cross-track displacement of the antennas, or "baseline", on the two passes is not zero, then the phase difference between two images will be related to the topography directly, as if there were two antennas mapping the scene simultaneously. Figure 3 shows a DEM generated from a spaceborne repeat-pass interferometer. In practice for repeat pass observations, part or all of the surface may change rapidly and completely, leading to no topographic information in an area.

One of the more exciting observations opened up by SAR interferometry occurs in repeat-pass systems when part of the imaged surface moves en masse in a coherent way. There is no sensitivity to topography in the phase difference between two antennas if the cross-track separation of the antennas is zero. However, a coherent motion of the surface between the two observation times will affect the phase difference directly and very sensitively. In this way, coherent motions at the scale of millimeters are easily measured from space. Usually the baseline is not zero, so there is also a component of topographic phase in the difference. This must be removed using an independent measure of the topography, either from an existing DEM, or using another interferometric observation pair between which no motion occurred. The pioneering demonstration of this technique was by Gabriel et al. [26] using SEASAT data mapping agricultural ground motions, but the technique became popular in 1993 after Massonnet et al. [27] demonstrated a spectacular signal from Landers 1992 earthquake. In Fig. 4, a differential interferometry map shows uplift of the San Fernando Valley, centered on the Santa Suzanna mountains, Los Angeles, CA.

A special case of repeat pass SAR interferometry is along-track interferometry, where two antennas are affixed to a single platform, displaced not cross-track but along-track. Thus the repeat interval for two observations is less than a second, and very fast motions can be imaged, such as water wave-patterns or vehicle motion. Actually, reports of along-track observations using the JPL AIRSAR system preceded spaceborne repeat pass observation reports. Goldstein and Zebker [28] augmented a conventional airborne SAR system with an additional aperture, separated along the length of the aircraft fuselage from the conventional SAR antenna, and showed that this system was capable of measuring tidal motions in the San Francisco bay area with an accuracy of several cm/s.

Interferometry continues to grow with new systems, such as SRTM operating as a ScanSAR interferometer, and RadarSAT-2, EnviSAT, ALOS, and LightSAR all with repeat pass interferometric and polarimetric capabilities. Future applications include global-scale topographic, tectonic and ice sheet mapping. In addition, the addition of polarimetry will greatly help to refine classification of land-cover, mapping of biomass, and hazard assessment capabilities.

V.FUTURERADAR

A. LightSAR

The primary science instrument planned for the LightSAR mission [14] is an L-band SAR. This instrument is specifically designed to meet NASA's science objectives for the mission, which include the use of repeat-pass interferometry to measure surface change, radar polarimetry to measure soil moisture, forest regeneration and snow wetness, and SCANSAR measurements to study mesoscale ocean circulation. In addition, a high-resolution imaging capability has been incorporated into the design to enhance the commercial potential for LightSAR data. The mission lifetime will be five years, to allow long observation timescales. Global access is also a feature of this mission. This means that LightSAR will be a free-flying, low earth orbit satellite, with a polar orbit. The orbit track will be tightly controlled to permit repeat-pass interferometry on every orbit repeat cycle. The radar will be able to look both sides of the spacecraft track, through a spacecraft roll maneuver. Combined with electronic steering of the antenna this will allow coverage of wide areas on each side of the spacecraft track. Taken together, these capabilities mean that LightSAR will be able to image any location on the earth's surface (and generate useful information) within a day of a significant event, which will provide a powerful capability for NASA's Natural Hazards program.

The LightSAR antenna will be an electronically steered, distributed, phased array which measures 10.8 x 2.9 meters. The antenna design has both H- and V-polarization, and can transmit up to 8 kW of RF power over a bandwidth of up to 80 MHz. The mass density, at less than 6 kg per square meter, is considerably less than that of comparable SAR antennas. This weight reduction in the design has been accomplished with a patch radiator element design with a panel thickness of just 1.38 cm, made up of a 1.27 cm thickness of low density honeycomb core and 0.55 mm glass/cyanate composite skins on each face to form panels of ample stiffness. The LightSAR RF and Digital electronics subsystems, which are housed within the spacecraft bus, are

also designed for very low weight and low power usage with high reliability and flexibility. Lightweight monolithic microwave integrated circuit (MMIC) technology are used in the RF subsystem design to achieve this. In the Digital Electronics subsystem, miniaturized FPGA-based designs have proven to give lower mass, reduced volume and better power efficiency than the components used on SIR-C, for example. The combined mass of the antenna, the RF and Digital electronics subsystems, which make up the radar instrument, is less than 300 kg. The DC power needed during radar data collection is less than 1200 W, and the peak data rate is less than 150 Mbps.

Critical aspects of the design and associated technologies have already been developed, tested, and validated using NASA/JPL's AIRSAR airborne testbed. AIRSAR is currently routinely collecting data with an L-band 80 MHz bandwidth fully polarimetric radar based on the same design and in many cases identical components and assemblies to those that will be used on LightSAR. An example of the 80 MHz AIRSAR image is shown in Fig. 5. Each of the operational modes for LightSAR shown in Figure 2 were successfully demonstrated during the two SIR-C missions in 1994. This includes the acquisition, processing and analysis of spotlight mode data, polarimetric SAR, ScanSAR and repeat-pass interferometry data.

The LightSAR radar instrument has been designed to provide the performance required to meet NASA's objectives, yet through the appropriate use of technology will cost less and have lower mass than comparable radar instruments. The benefits of this approach to the LightSAR program are that it lowers the cost of the launch vehicle and allows the instrument to fly on a lower cost, readily available spacecraft bus. The LightSAR mission reverses the trend for increasing mass, cost and complexity in spaceborne SAR instruments. It can be regarded as a step along the road to the next generation of SAR systems, which will use antennas of even lower mass, possibly inflatables, lightweight, more efficient deployment structures and electronics. The success of LightSAR, with its reduced number of modes (relative to SIR-C, for example) will help forge a path towards more focused, long-term measurements using an even smaller number of modes. It will also demonstrate that future SAR instrument which fly on NASA missions will not take up all the platform resources, i.e. mass allocation, power availability, data storage or data transmission.

B. Beyond LightSAR

This section discusses the characteristics of future science SAR missions beyond LightSAR, which are likely to be launched after 2002. Based on current study activities, the future SAR missions will be noticeably different from the previous missions. For SAR to be competitive with other remote sensing instruments, the SAR mission cost must be drastically reduced. In order to lower the mission cost, it is necessary to utilize advanced radar technologies for constructing the lighter weight and more power efficient SAR hardware. In addition, most future SAR missions will be designed for focused science objectives based on the experience from previous experimental SAR missions such as the shuttle imaging radar series. The involvement of commercial companies is expected to be expanded to many areas of the mission operation. The collected data may be processed either on-board or by the users in distributed facilities instead of a centralized processing facility. Finally, more SAR data will be used together with other remote sensing data for various GIS (Geographic Information System) applications.

In order to provide the volume of remote sensing data to meet future science requirements, it may be necessary to deploy many SAR instruments for various science objectives. However, this SAR constellation may not be realized without further reducing the mission cost. To reduce the mission life-cycle-cost, it is necessary to reduce the weight of the SAR instrument using advanced technologies. Since the antenna weight is usually more than half of the entire radar mass especially with the complicated deployment mechanism, the SAR antenna is the prime candidate for implementing radically different technology. The antenna physical size must be large enough to obtain the necessary SNR because the transmit power is limited in the space environment. For a typical L-band SAR, the physical antenna area is approximately 30 m^2. The most promising approach for significantly reducing the antenna mass is the use of space inflatable structures to deploy the antenna and to provide the antenna structure [29]. Microstrip radiation elements are etched on the conductor-dielectric layer thin-film membrane surface in order to fold it within a small volume. The expected mass density is less than 3 kg/m^2 which includes the aperture, structure, inflation system and T/R modules. This is a significant improvement when it is compared with the SIR-C antenna density of 23 kg/m^2 for L-band antenna panel alone without the sturucture. The inflatable antenna deployment sequence is illustrated in Fig. 6.

The radar electronics and T/R modules will be efficient in power consumption to reduce the weight and complexity associated with the solar panel and other power related subsystems. As an example, the future single channel L-band radar electronics consumes less than 50 W. The radar electronic will be miniaturized by using advanced technologies such as MMIC, MEMS, SAW device, ASIC, and FPGA technology. The expected weight of a single channel L-band radar

electronics will be less than 15 kg and the entire volume will be less than 10" x 12" x 9". The radar electronics will be designed to be easily integrated with the spacecraft hardware.

Based on experience from previous experimental SAR instruments and airborne test-beds, future SAR missions will be designed to satisfy focused science objectives. As an example, it is well known that radar interferometry has the unique capability to measure the small-scale change (mm to cm) caused by natural hazards such as earthquakes. This technique has been demonstrated by using repeat track SAR data from various space-borne radar sensors such as SEASAT, SIR-C, ERS, JERS, and RadarSAT. Therefore, the clear next step is to develop an operational system to monitor the surface changes to mitigate the potential hazards. The L-band SAR was recommended by the radar science community for this application to minimize the temporal decorrelation effect. The atmospheric disturbance must be compensated for minute surface change detection. Another example is the L-band polarimetric SAR for the global soil moisture mapping. The basic concept of this mission has been demonstrated by using the airborne and the SIR-C data. The required resolution is approximately 1 km to satisfy the science and repeat coverage requirements. A P-band polarimetric SAR can be used for the global biomass estimation. In order to implement this concept, we need to develop a technique to compensate ionospheric effects. All these operational instrument will deliver the global science data every 2-3 days.

Since the data volume associated with the SAR instrument is extremely high, the requirement for the data downlink system is very demanding. Unlike optical images, SAR raw data cannot be compressed since it is a Gaussian noise. Therefore, to reduce the downlink data rate significantly, the future SAR may utilize on-board processing technology. If the ground processing option is implemented, data users will be able to process at their location instead of relying on a centralized processing facility. In addition to the data processing technology, it is necessary to advance geophysical information extraction algorithms. Especially, the global application of these radar science algorithms must be verified. In the future, the best use of the SAR data will be realized when it is combined with other remote sensing data through data fusion techniques.

VI.SUMMARY

The evolution of imaging radar technology has been dramatic over the past 50 years, building from the developments of World War II. Early side-looking airborne radars served as developmental platforms from which to launch to space. The development of the synthetic

aperture technique, where the radar resolution is independent of the platform altitude, was a key step to high resolution space-borne imaging radars. The many developments in flight radar equipment, digital processing capabilities and remote sensing techniques have enabled the sophisticated systems of today. The intrinsic radar capability to "see" through darkness, clouds, and smoke is now being utilized from space to cover large areas rapidly and produce global geological and topographic maps. Using advanced SAR techniques such as polarimetry and interferometry, civilian space-borne imaging radar systems can produce more accurate elevation mapping, natural hazards monitoring, soil moisture mapping and biomass estimation. As technology continues to advance and to make space-borne radar missions more affordable, future SAR missions have the capacity to revolutionize remote sensing of Earth's surface.

REFERENCES

[1] Skolnik, M. I., *Introduction to Radar Systems*, McGraw-Hill, New York, 1980.

[2] Elachi C., *Spaceborne Radar Remote Sensing: Applications and Techniques*, IEEE press, New York, 1988

[3] Curlander, J. C. and R. N. McDonough, *Synthetic Aperture Radar Systems and Signal Processing*, John Wiley & Sons, New York, 1991.

[4] Ulaby, F. T. and C. Elachi ed., *Radar Polarimetry for Geoscience Applications*, Artech House, MA, 1990.

[5] Handerson, F. M. and A. J. Lewis ed., *Principles & Applications of Imaging Radar*, Manual of Remote Sensing, Third Edition, Volume 2, John Wiley & Sons, New York, 1998.

[6] Peltzer, G. and P. Rosen, "Surface Displacement of the 17 May 1993 Eureka Valley, California, Earthquake Observed by SAR Interferometry," *Science*, Vol. 268, pp. 1333-1336, 1995.

[7] Wiley C. A., "Synthetic Aperture Radars – a Paradigm for Technology Evolution," *IEEE Trans. Aerospace Elec. Sys.*, AES-21, pp. 440-443, 1985.

[8] Porcello, L. J. et al. "The Apollo Lunar Sounder System," *Proc. IEEE*, Vol.62 pp 769-783,1974.

[9] Granger, J. L. "Shuttle Imaging -- A/B Sensors" in Spaceborne Imaging Radar Symposium. Pasadena, Calif. Jet Propulsion Laboratory Pub 83-11 July 1, 1983.

[10] Elachi, C. E. "Spaceborne Synthetic Aperture Imaging Radars: Applications, Techniques, and Technology," *Proc. IEEE*, Vol 70, 1982.

[11] Johnson, W.T.K., "Magellan Imaging Radar Mission to Venus," *Proc. IEEE*, Vol 79, pp. 777-790, 1991.

[12] Jordan, R. L, B. L. Huneycutt, and M. Werner, "The SIR-C/X-SAR Synthetic Aperture

Radar System," *IEEE Trans. Geosci. Remote Sens.*, GRS-33, pp. 829-839, 1995.

[13] Elachi, C. et al., "RADAR: The Cassini Titan Radar Mapper," submitted for publication, 1999.

[14] Hilland, J. E., Stuhr, F. V., Freeman, A., Imel, D., Shen, Y., Jordan, R. and Caro, E., Future NASA Spaceborne SAR Missions, *IEEE-AES Systems Magazine*, Vol. 13, No. 11, November 1998.

[15] Attema, E. W. P., "The Active Microwave Instrument On-board the ERS-1 Satellite," *Proc. IEEE*, Vol. 79, pp. 791-799, 1991.

[16] Nemoto, Y. et al., "Japanese Earth Resources Satellite-1 Synthetic Aperture Radar," *Proc. IEEE*, Vol. 79, pp. 800-808, 1991.

[17] Luscombe, A.P., I. Ferguson, N. Shepherd, D. G. Zimcik, and P. Naraine, "The RadarSAT Synthetic Aperture Radar Development, " *Canadian Journal of Remote Sensing*, Vol. 19, pp. 298-310, 1993.

[18] Zebker, H. A., J. J. van Zyl and D. N. Held, "Imaging Radar Polarimetry from Wave Synthesis," *J. Geophys. Res.*, 92, pp. 683-701.

[19] van Zyl, J. J., "A Technique to Calibrate Polarimetric Radar Images Using Only Image Parameters and Trihedral Corner Reflectors," *IEEE Trans. Geosci. Remote Sens.*, GRS-28, pp. 337-348, 1990.

[20] Freeman, A., SAR Calibration: An Overview, *IEEE Trans. on Geosci. Remote Sens.*, GRS-30, No. 6, pp. 1107-1121, 1992.

[21] Oh, Y. K. Sarabandi, and F. T. Ulaby, "An Empirical Model and an Inversion Technique for Radar Scattering from Bare Soil Surfaces," *IEEE Trans. Geosci. Remote Sens.*, GRS-30, pp. 370-381, 1992.

[22] Dubois, P. C. J. J. van Zyl, and T. Engman, "Measuring Soil Moisture with Imaging Radars," *IEEE Trans. Geosci. Remote Sens.*, GRS-33, pp. 915-926, 1995.

[23] Graham, L. C., "Synthetic Interferometric Radar for Topographic Mapping," *Proc. IEEE*, Vol. 62, no. 6, pp. 763-768, 1974.

[24] Zebker, H. A. and R. M. Goldstein, "Topographic mapping from interferometric SAR observations," *J. Geophys. Res.*, 91, pp. 4993-4999, 1986.

[25] F. Li and R. M. Goldstein, "Studies of multibaseline spacborne interferometric synthetic aperture radars," IEEE Trans. *IEEE Trans. Geosci. Remote Sens.*, GRS-28, pp. 88-97, 1990.

[26] Gabriel, A. K., R. M. Goldstein, and H. A. Zebker, "Mapping small elevation changes over large areas: Differential radar interferometry." *J. Geophys. Res.*, 94, pp. 9183-9191, 1989.

[27] Goldstein, R. M. and H. A. Zebker, "Interferometric radar measurement of ocean surface currents," *Nature*, vol. 328, pp. 707-709 1987.

[28] Massonnet, D., M. Rossi, C. Carmona, F. Adragna, G. Peltzer, K. Fiegl, and T. Rabaute,

"The displacement field of the Landers earthquake mapped by radar interferometry," *Nature*, vol. 364, pp. 138-142, 1993.

[29] Huang, J., M. Lou, A. Feria, and Y. Kim, " An Inflatable L-Band Microstrip SAR Array," *IEEE APS/URSI Symposium*, Atlanta, Georgia, June 1998.

FIGURECAPTIONS

Figure 1. Full resolution mosaic Magellan image in the Lavina region of Venus. Three large impact craters can be seen in a region of fractured plains. The craters show many features typical of meteorite impact craters, including rough, radar-bright ejecta, terraced inner walls and central peaks.

Figure 2. LandSAT (left) and SIR-C (right) images of the area surrounding Sunbury, Pennsylvania in the Appalachian Valley and Ridge province, formed when the Appalachian mountains were formed some 370 to 390 million years ago. The river junction is where the West Branch river flows into the Susquehanna River. The valleys provide fertile farmland shown in blue in the radar image. The more resistant rocks, such as sandstone, form the top of the ridges which appear as forest greenish areas on the radar image. The cross-polarized radar channel, displayed in green, clearly responds very strongly to the presence of vegetation, displaying the strong sensitivity to biomass.

Figure 3. Digital elevation model generated from SIR-C radar data in October 1994. On two orbits separated by two days, radar data were acquired over a stretch of land from the California-Oregon border down to Mexico. The images were combined by the methods of interferometry to produce this height product. Note that the radar imagery are automatically geocoded and overlaid as brightness variations on the color-coded elevation data. The accuracy of the product varies from a few meters error in the best areas (bright return, low slopes) to 10-15 m in the noisy (dark, sloped) areas. The resolution of this product is about 100 m.

Figure 4. Map showing uplift of the San Fernando Valley, centered on the Santa Suzanna mountains, Los Angeles, CA. Uplift was caused by the 1994 M=6.7 Northridge earthquake. The map was generated using radar data acquired on two passes of the JERS-1 satellite separated by three months surrounding the event. The topographic component of the interferometric phase was removed using a known digital elevation model provided by the USGS. Uplift of 60 cm with accuracy of about 5 mm is seen. Gray brightness variations are superposed on the color-coded deformation to show geologic features in the Los Angeles area. Areas without color are those for which the estimate of deformation was too noisy, either from surface disruption, interferometric imaging limitations, or elevation model inaccuracies.

Figure 5. This image shows an inland portion of Manatee and Sarasota counties in southeastern

Florida, east of the city of Sarasota. The area shown in this radar image is 25 km (16 miles) inland to the east from the Gulf of Mexico. Numerous rivers in this region, including the Manatee, Braden and Myakka Rivers drain towards the Gulf. These rivers and the many small lakes (dark regions in the radar image) are evidence of the porosity of the limestone rock that underlies much of Florida.

Figure 6. Inflatable antenna deployment sequence. (a) stowed membrane inflatable antenna, (b) partially inflated membrane inflatable antenna, (c) fully inflated and rigidized membrane inflatable antenna.

Sunbury, Pennsylvania

40.86 deg N, 76.79 deg W

October 30th, 1984

LANDSAT Color Overlay
2.08 - 2.35 μm: Red
1.55 - 1.75 μm: Green
0.52 - 0.60 μm: Blue

October 6th, 1994

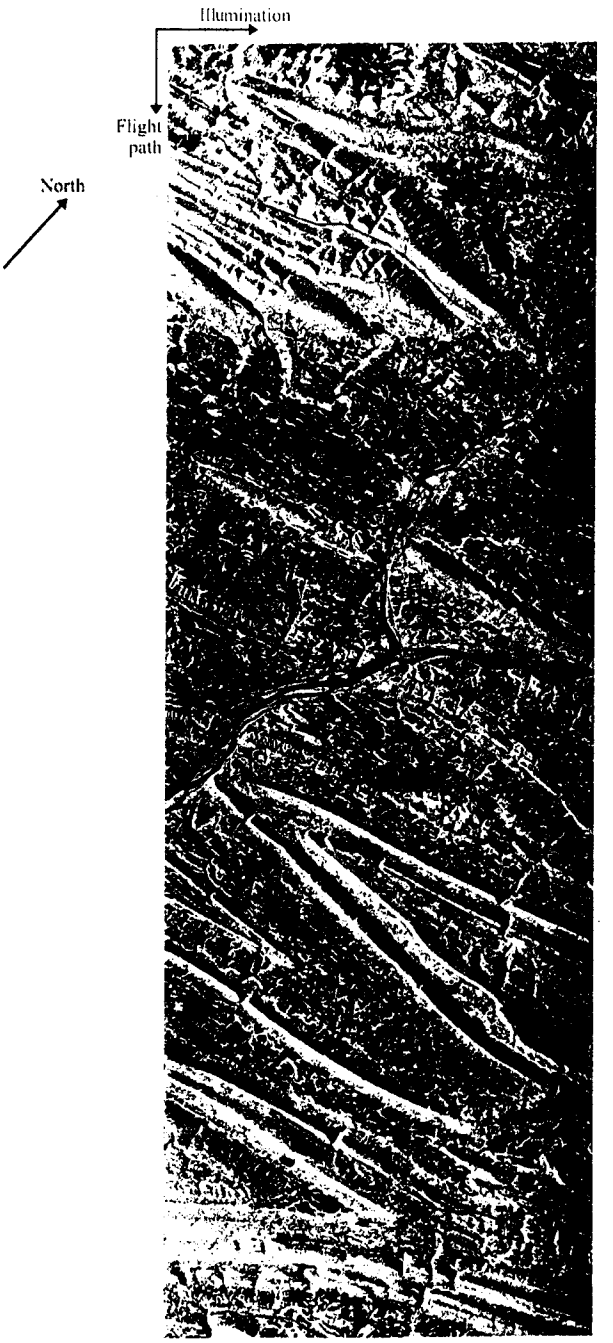

SIR-C Color Overlay
L-band, HH pol: Red
L-band, HV pol: Green
C-band, HH pol: Blue
Incidence angle: 38.6 deg

10 km

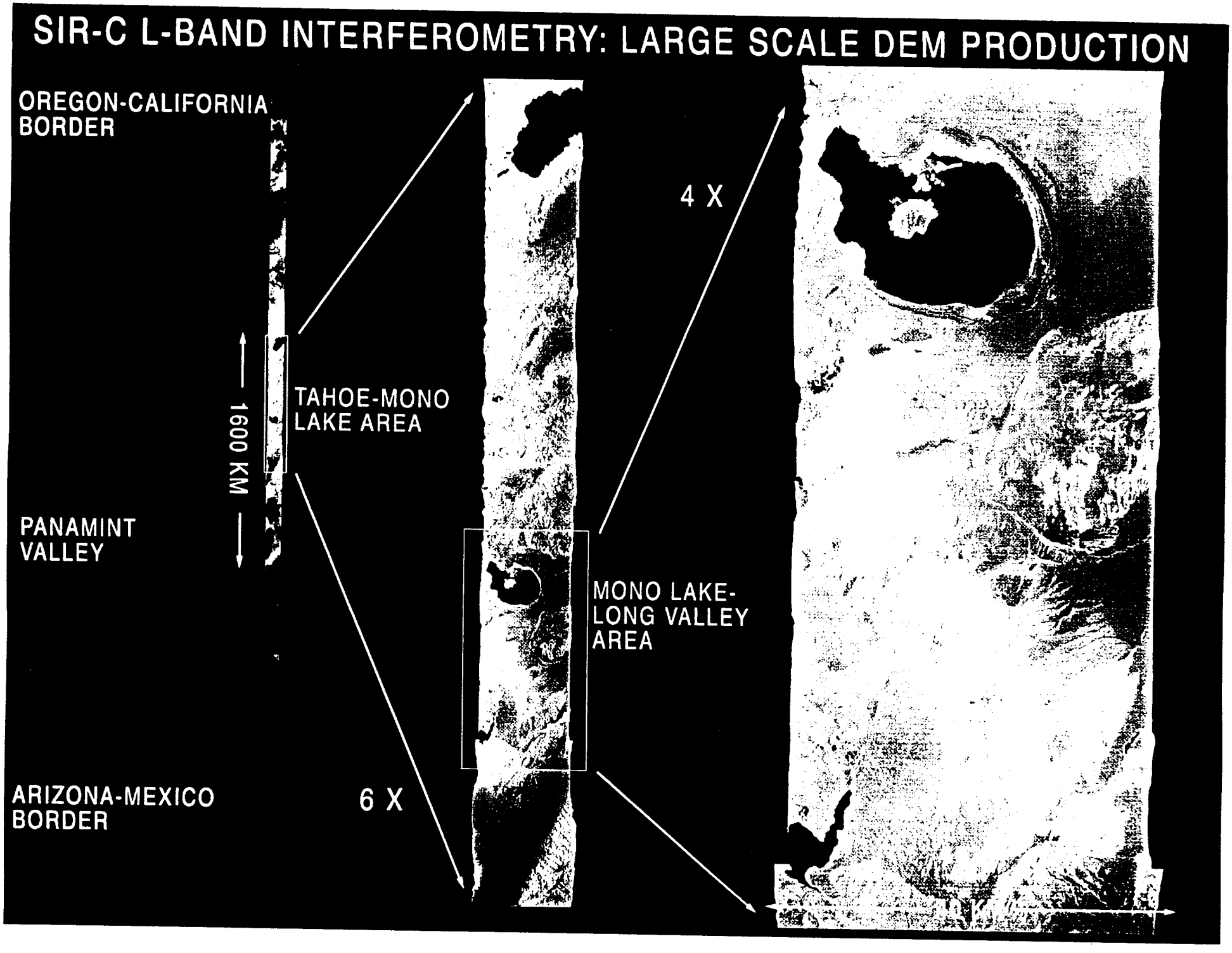
SIR-C L-BAND INTERFEROMETRY: LARGE SCALE DEM PRODUCTION
OREGON-CALIFORNIA BORDER
1600 KM
TAHOE-MONO LAKE AREA
PANAMINT VALLEY
ARIZONA-MEXICO BORDER
6 X
MONO LAKE-LONG VALLEY AREA
4 X

SURFACE DISPLACEMENTS OF THE 1994 NORTHRIDGE M6.7 EARTHQUAKE

JERS-1 TWO-PASS RADAR INTERFEROMETRY

JPL

Rosen et al. 1995

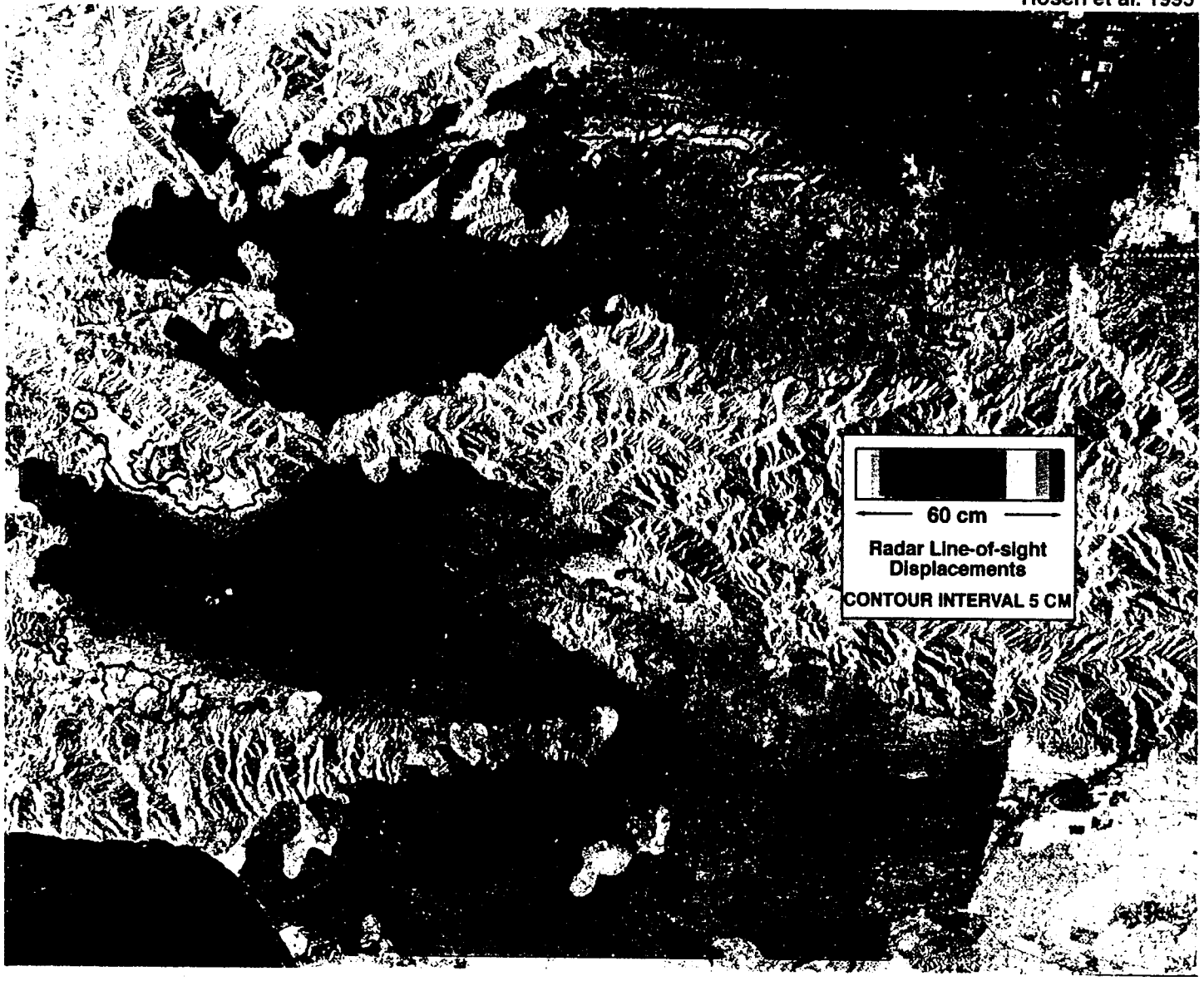

INTEGRATED AIRSAR PROCESSOR (V. 6.10)

MANATEE 9LOOK

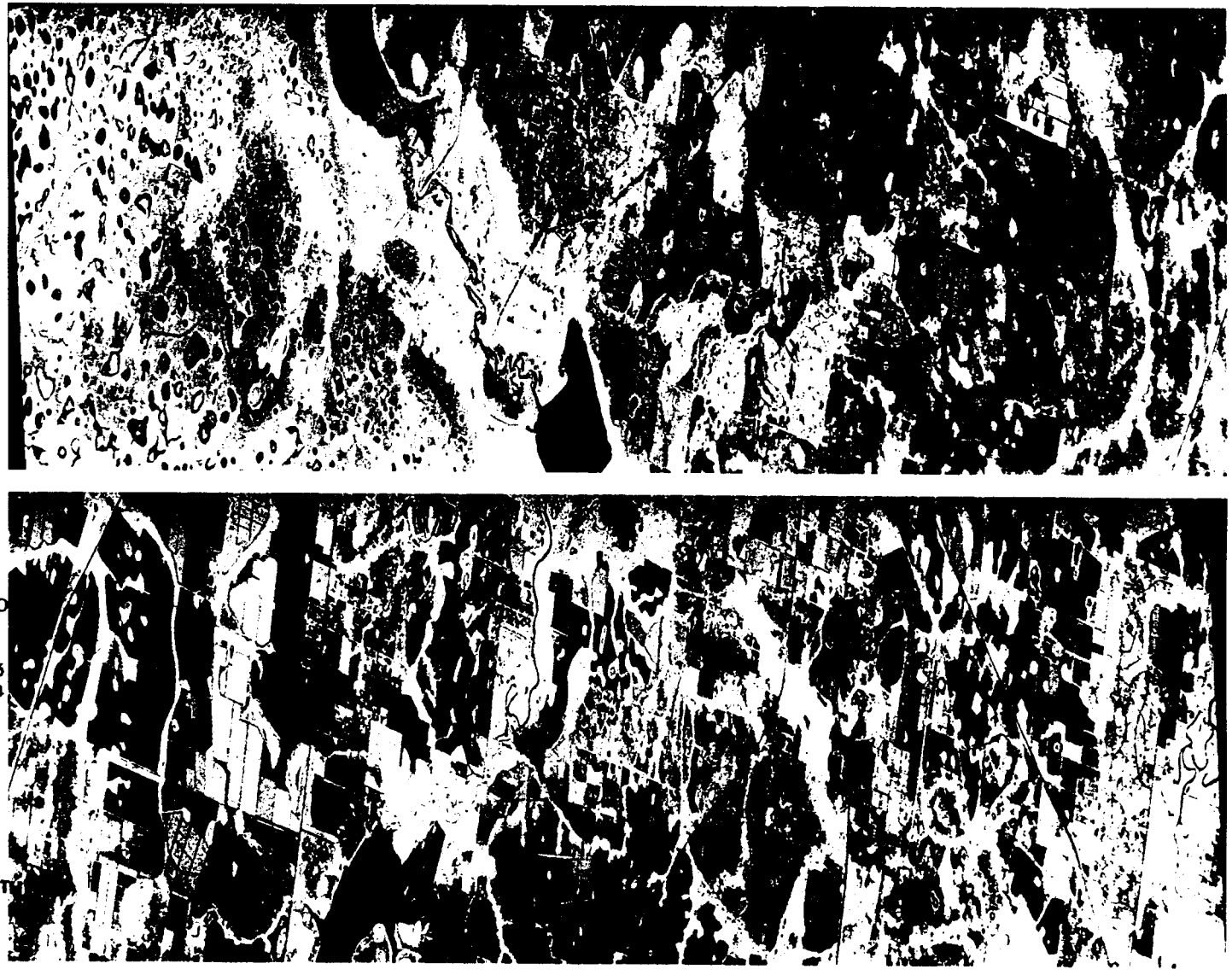

L-Band HH
L-Band HV
L-Band VV

Date Acquired:
29-OCT-98
Date Processed:
11-DEC-98
CCTID: CM5478

Cntr lat: 27.45
Cntr lon: -82.36
Bandwidth: 80.00
Cross-track:
swath(km): 4.2
samples in data: 2560
reduction ratio: 0.2
Along-track:
swath(km): 59.3
lines in data: 12854
reduction ratio: 0.2

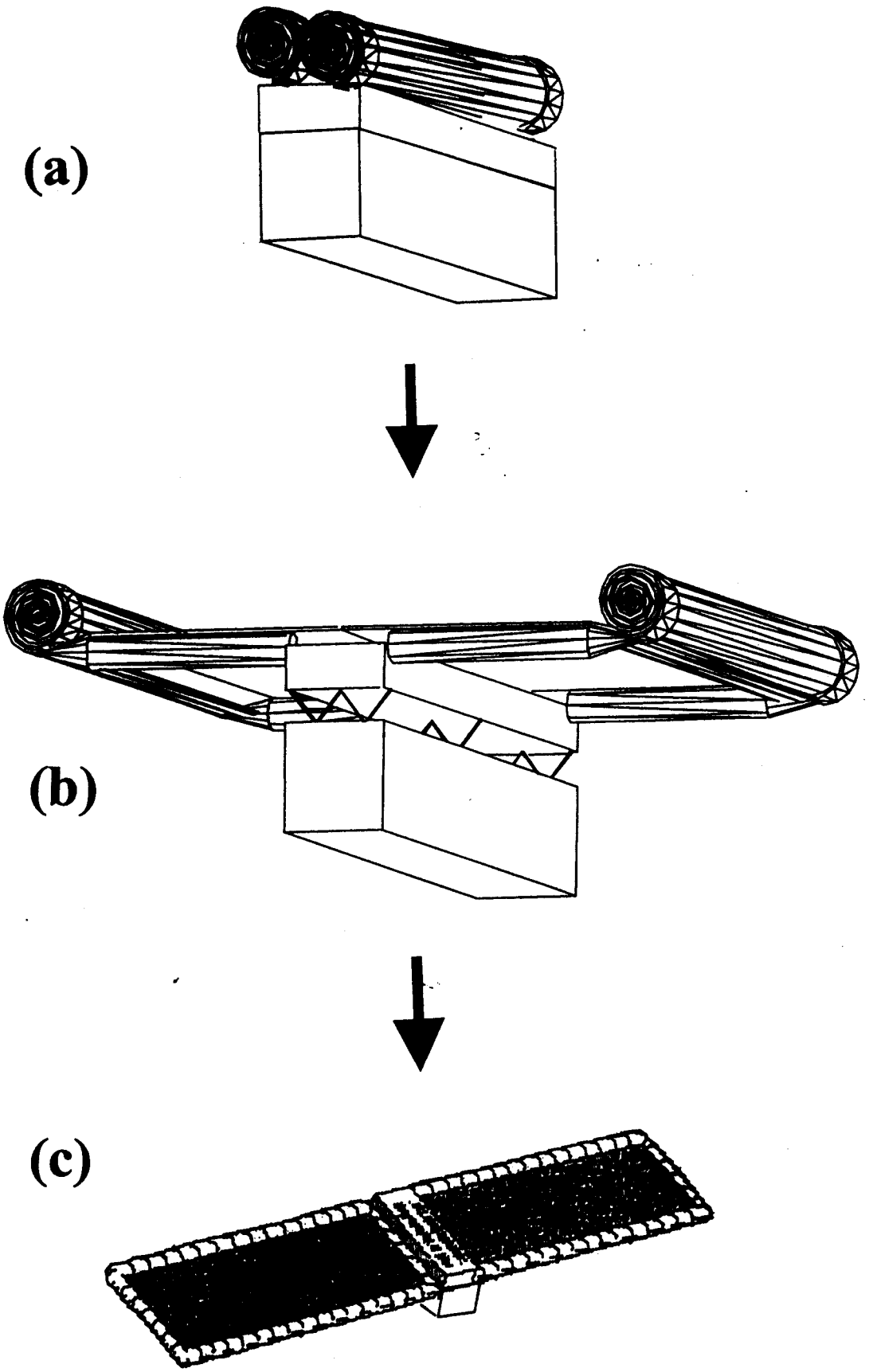
(a)
(b)
(c)